PAPER

Recovery of copper/carbon matrix nanoheteroarchitectures from recyclable electronic waste and their efficacy as antibacterial agents

Mariam M. Abdelkhalek,[a] Rania Seif,[a] Rehab Z. Abdallah, [b] Abdallah A. Akar,[a] Rania Siam[b] and Nageh K. Allam [*a]

Innovative solutions are urgently needed with the growing environmental hazard of electronic waste (e-waste) and the rising global threat of bacterial infections. This study addresses both issues by using e-waste to produce copper nanoparticles within a carbon matrix (Cu/C NPs), mitigating environmental hazards while exploring their antibacterial properties. Printed circuit boards from discarded computers were collected and treated with 2 M ammonium citrate dissolved in 8% ammonia solution. The leached solution was used to synthesize copper particles using ascorbic acid. The synthesized Cu/C NPs were characterized using various techniques such as EDX, field-emission scanning electron microscopy (FESEM), transmission electron microscopy (TEM), X-ray diffraction (XRD), and Fourier transform infrared (FT-IR) spectroscopy. The antibacterial activity of Cu/C NPs against *Escherichia coli* (*E. coli*) and *Staphylococcus aureus* (*S. aureus*) was evaluated using colony-forming unit (CFU) reduction assay and calculating the minimum inhibitory concentrations (MICs). The Cu/C NPs were found to be effective against *E. coli* and *S. aureus* with 100% and 98% CFU reduction, respectively, with MICs ranging from 250 to 375 μg mL^{-1} for *E. coli* and 375 to 750 μg mL^{-1} for *S. aureus*, according to the bacterial load. The bactericidal kinetics showed complete bacterial elimination after 5 and 7 hours for *E. coli* and *S. aureus*, respectively. This study presents a sustainable approach for utilizing e-waste and demonstrates the potential of the recovered nanoparticles for antibacterial applications.

1. Introduction

The rapid advancement of information and communication technology and the increasing production of electronic products have led to a significant rise in the amount of electronic waste, commonly known as e-waste.[1] This growing e-waste generation poses significant environmental challenges worldwide.[2,3] According to a report from 2019, the global generation of e-waste reached 53.6 million tons, showing a 21% increase since 2015.[1,4] As much as 83% of this e-waste was undocumented and mostly improperly disposed of, leading to severe consequences for public health and the environment. Only 17% of the e-waste was properly collected and recycled.[3] Although electrical and electronic devices contain a range of toxic substances, they also encompass significant quantities of valuable precious metals that should not be overlooked.[5] Toxic components in e-waste include heavy metals and hazardous

substances such as lead, nickel, antimony, mercury, cobalt, thallium, cadmium, beryllium, polyvinyl chloride, and brominated flame retardants. Conversely, e-waste is rich in precious and base metals like silver, gold, copper, and palladium. This makes e-waste a valuable secondary resource for the recovery of metals at low operating costs.[3,6] Among the various methods of extraction of precious metals from e-waste, hydrometallurgical processes are known for their adaptability during scaling-up and management procedures. They are often considered more environmentally friendly and less energy-intensive compared to alternative methods for recycling waste printed circuit boards (WPCBs).[3,6] The extraction and development of nanomaterials from e-waste has opened up new application possibilities, including their use as antibacterial agents.[7]

The exploration of unconventional antibacterial agents is emerging as a significant area of research.[8–10] In particular, there has been a growing focus on inorganic bactericides due to their effectiveness, stability, and ability to withstand high temperatures.[11,12] The US Environmental Protection Agency acknowledged copper and its compounds as materials with antimicrobial properties.[13,14] The antimicrobial properties of bulk copper have been utilized for food preservation and water sanitization since the

aEnergy Materials Laboratory, Physics Department, School of Sciences and Engineering, The American University in Cairo, New Cairo 11835, Egypt. E-mail: nageh.allam@aucegypt.edu

bDepartment of Biology, School of Sciences and Engineering, The American University in Cairo, New Cairo 11835, Egypt

ancient eras.[15] The advancement of nanoscience and nanotechnology has opened up new possibilities for investigating the antimicrobial properties of innovative nanomaterials that incorporate bioactive metals like silver, copper, titanium, and zinc.[16–18] Copper, in particular, has been extensively studied for its antimicrobial activity due to its affordability, biocompatibility and flexible synthesis techniques[15,19,20] When diminished to the nanoscale, copper nanoparticles (CuNPs) have found use in a range of antibacterial applications such as food packaging, antibacterial coatings, and skin products.[15,21,22] Several studies have been conducted to explore the antibacterial properties of elemental copper and its oxides in relation to factors such as particle size, shape, and the release of copper ions in different environments.[23,24]

Herein, a novel approach is demonstrated that involves the successful extraction and synthesis of elemental copper nanoparticles in carbon matrix (Cu/C NPs) from WPCBs, bypassing the conventional use of costly chemical substances. This innovative method is cost-effective and offers a unique solution for handling e-waste. Leveraging this approach not only addressing environmental concerns associated with chemical extraction processes but also opening up new possibilities for the reclamation of valuable materials from e-waste. The cost-effectiveness of this method could make it more accessible and scalable for widespread implementation, leading to a more sustainable approach to managing e-waste in the future. This method not only offers a sustainable solution but also enhances the environmental appeal of our material. We conducted comprehensive characterization of the material using EDX, transmission electron microscopy (TEM), field-emission scanning electron microscopy (FESEM), Fourier transform infrared (FT-IR) spectroscopy, Raman spectroscopy, and X-ray diffraction (XRD) analyses. The antibacterial properties of the Cu/C NPs were thoroughly evaluated against both *Escherichia coli* (*E. coli*) and *Staphylococcus aureus* (*S. aureus*) by CFU reduction assay, minimum inhibitory concentrations (MICs) at different bacterial burdens, and bactericidal kinetics.
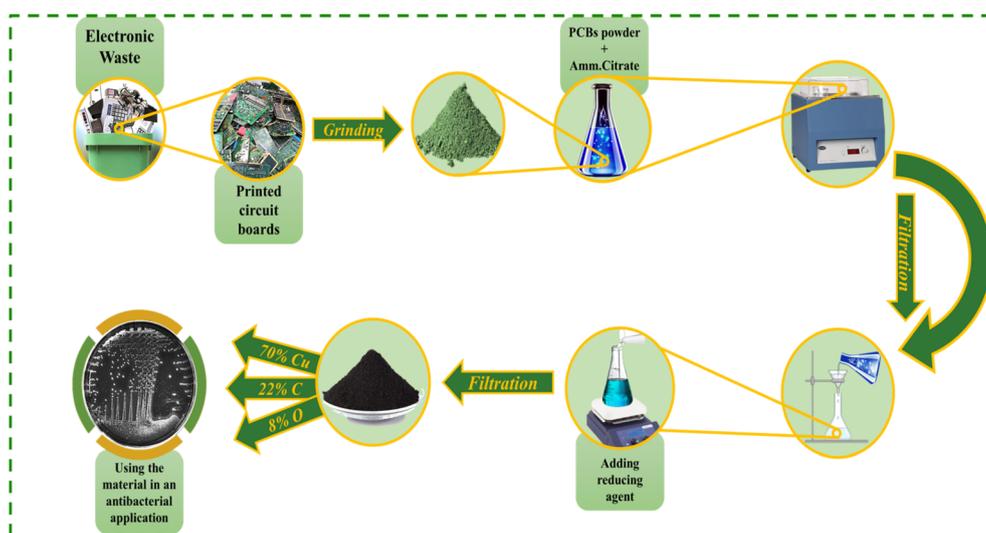
2. Materials and methods

2.1 Materials and chemicals

WPCBs of discarded computers were collected from different electronic shops in Cairo. Ammonium citrate ($C_6H_{17}N_3O_7$), ammonia solution (25% NH_3), and ascorbic acid ($C_6H_6O_8$) were purchased from Alfa-Aser. Luria–Bertani (LB) broth (Difco), LB agar (Difco), phosphate buffer saline (PbS, Sigma-Aldrich), and resazurin dye (Loba) were used. *E. coli* and *S. aureus* were used as model Gram-negative and Gram-positive organisms, respectively. All chemicals were used without further purification. The water used in the preparation steps was deionized water from the ultrapure water system, Millipore Direct-Q3 with UV.

2.2 Preparation of Cu/C NPs

2.2.1 Leaching experiments. 2 kg of discarded WPCBs from computers were shredded and grinded to reduce the size to approximately 0.6 mm powder. WPCB powders were used for the leaching experiments without any further treatment. The experiment was carried out in a water bath adjusted at 80 °C. 2 g of WPCBs was leached by 2 M of ammonium citrate dissolved in 8% ammonia solution with a solid : liquid ratio of (1 : 20) for 3 h, followed by filtration. The extracted filtrate was used to synthesize nanoparticles, as represented in Scheme 1.

2.2.2 Synthesis of the Cu/C NPs. Cu/C NPs nanoparticles have been synthesized using a solution-based co-precipitation method. Ascorbic acid was added drop by drop to 250 mL of leached solution. The whole process was carried out at 70 °C. After two days, the solution turned dark brown. The precipitated material was collected by filtration and washed several times with deionized water, followed by alcohol to remove unreacted ions. After that, the as-precipitated material was dried in a vacuum oven at 60 °C. The synthesized nanoparticles were characterized successfully using XRD, Raman, FTIR, EDX, SEM, and TEM. The surface morphology of the Cu/C NPs nanoparticles was assessed *via* a Zeiss Ultra 60 FESEM. X-ray

Scheme 1 The synthesis process of Cu/C NPs from e-waste.

diffractometer on an X'Pert PRO MRD with Cu-kα radiation (λ = 0.15406 nm) was utilized to inspect the crystal structure. The structural functional groups were verified from the executed FTIR absorption curves in the 400–4000 cm^{-1} range *via* an ATI Unicam (Mattson 936) benchtop spectrometer using pressed KBr pellets.

2.2.3   Preparation of Cu/C NPs suspension. Cu/C NPs were UV sterilized for 20 minutes, then suspended in distilled sterilized water to a concentration of 4 mg mL^{-1} and homogenized by ultrasonication for 15 seconds. The suspension was then diluted with distilled sterilized water to reach lower concentrations which were used in subsequent tests (CFU reduction, MICs determination, and time–kill curves).

2.3   Antibacterial assays

2.3.1   Preparation of bacterial inocula. CLSI recommendations for the preparation of bacterial suspension were followed; *E. coli* suspension was prepared using the growth method, whereas *S. aureus* inocula was prepared by the colony suspension method.[25] Pure plates of both organisms on LB agar were prepared. In the case of *S. aureus*, identical colonies were suspended in LB broth until OD$_{600}$ was adjusted to the required value. On the other hand, a single separate colony of *E. coli* was suspended in LB broth and incubated overnight at 37 °C. Consequently, OD$_{600}$ was measured and calibrated as required.

2.3.2   Screening of antibacterial activity of Cu/C NPs. To screen the antibacterial activity of Cu/C NPs, both *E. coli* and *S. aureus* (1×10^6 to 1×10^7 CFU mL^{-1}), were incubated in the presence of a preliminary concentration of Cu/C NPs (500 μg mL^{-1}). Positive control tubes containing the same concentrations of bacteria without Cu/C NPs were also prepared. Sterility control tubes containing 500 μg mL^{-1} of Cu/C NPs in LB broth and negative control tubes containing only LB broth were additionally prepared. All tubes were then incubated in a shaking incubator at 180 rpm for 24 hours at 37 °C. Consequently, the tubes were serially diluted and spread on LB agar. The plates were incubated for 24 hours at 37 °C. Colony counts were then recorded. All experiments were done in triplicates, and means were calculated. The percentage of inhibition was calculated using eqn (1):

$$\text{Inhibition percentage} =$$

$$\frac{\text{CFU mL}^{-1} \text{ of positive control} - \text{CFU mL}^{-1} \text{ of test sample}}{\text{CFU mL}^{-1} \text{ of positive control}} \quad (1)$$

2.3.3   Minimum inhibitory concentrations (MICs). MICs of Cu/C NPs against both *E. coli* and *S. aureus* were determined by plate microdilution method in 96-well plates. MICs were determined at three bacterial concentrations for each organism; high bacterial load (1×10^6 to 1×10^7 CFU mL^{-1}), intermediate bacterial load (5×10^4 to 5×10^5 CFU mL^{-1}), and low bacterial load (1×10^3 to 1×10^4 CFU mL^{-1}). The bacteria were incubated with concentration gradients of Cu/C NPs. One column was assigned as a negative control, containing only LB broth, while another column functioned as a positive control,

comprising only bacterial inocula without Cu/C. Each plate also contained a sterility control row containing serial dilutions of Cu/C NPs without bacteria. The bacterial inocula and the Cu/C NPs suspension were vortexed before pipetting. Plates were incubated in a shaking incubator at 180 rpm for 18 hours at 37 °C. All experiments were done in triplicates. Resazurin dye was dissolved in sterile PBS (0.1 mg mL^{-1}) and sterilized *via* 0.22 μm syringe filter. The dye solution was freshly prepared and used on the same day. 50 μL of the resazurin solution was pipetted into every occupied well in the 96-well plate. Plates were then incubated for 75 minutes at 37 °C at 180 rpm.[26] After the second incubation period, the color change was observed; wells with unchanged blue dye color were considered negative for bacterial growth, whereas a change in the dye color to purple or pink was an indicator of bacterial growth.

2.4   Time–kill curve

Bacterial suspensions of 1×10^3 to 1×10^4 CFU mL^{-1} concentration were incubated with 1000 μg mL^{-1} Cu/C ($4 \times$ MIC for *E. coli* and $\sim 3 \times$ MIC for *S. aureus*). Positive control tubes containing the same concentrations of the bacteria without Cu/C NPs were prepared. Sterility control tubes containing 1000 μg mL^{-1} of Cu/C NPs in LB broth and negative control tubes containing only LB broth were additionally prepared. All tubes were incubated in a shaking incubator at 180 rpm at 37 °C. At each time point, samples were withdrawn from each tube, serially diluted, and spread on the surfaces of LB agar plates. The plates were incubated for 24 hours at 37 °C. Colony counts were then recorded. All experiments were conducted in triplicate, with the exception of *S. aureus* treated with Cu/C NPs, which was performed in duplicate. Mean values and standard deviations were computed and graphically presented.

3.   Results and discussion

3.1   Characterization of the recycled Cu/C NPs

The FESEM imaging of the Cu/C NPs sample showed well-defined, uniform spherical nanoparticles, where copper is embedded in a core–shell structure within carbon at a size of ~ 50 nm, Fig. 1(a and b). The elemental composition and distribution throughout the sample were propped using energy-dispersive X-ray (EDX) spectroscopy (Table 1). The EDX spectrum (Fig. 1c) revealed the presence of 70% copper, 22% carbon, and 8% oxygen. Also, the EDX mapping of the nanospheres (Fig. 1d–f) revealed good distribution of all elements in the sample. The XRD spectra (Fig. 1g) exhibited prominent peaks at 43.4°, 50.67°, and 89.9°, corresponding to the (111), (200), and (220) planes, respectively, with *d*-spacings of 2.08, 1.8, and 1.27. These peaks align with the body-centred cubic structure of metallic copper [(JCPDS 01-070-3039)]. Moreover, the absence of peaks corresponding to copper oxide in the XRD patterns may reveal the synthesis of pure metallic copper.[27] The calculated average grain size is found to be 13.53 nm.

The high-resolution transmission electron microscopy (HRTEM) images of the Cu/C NPs are depicted in Fig. 2. The TEM analysis revealed the formation of dispersed Cu
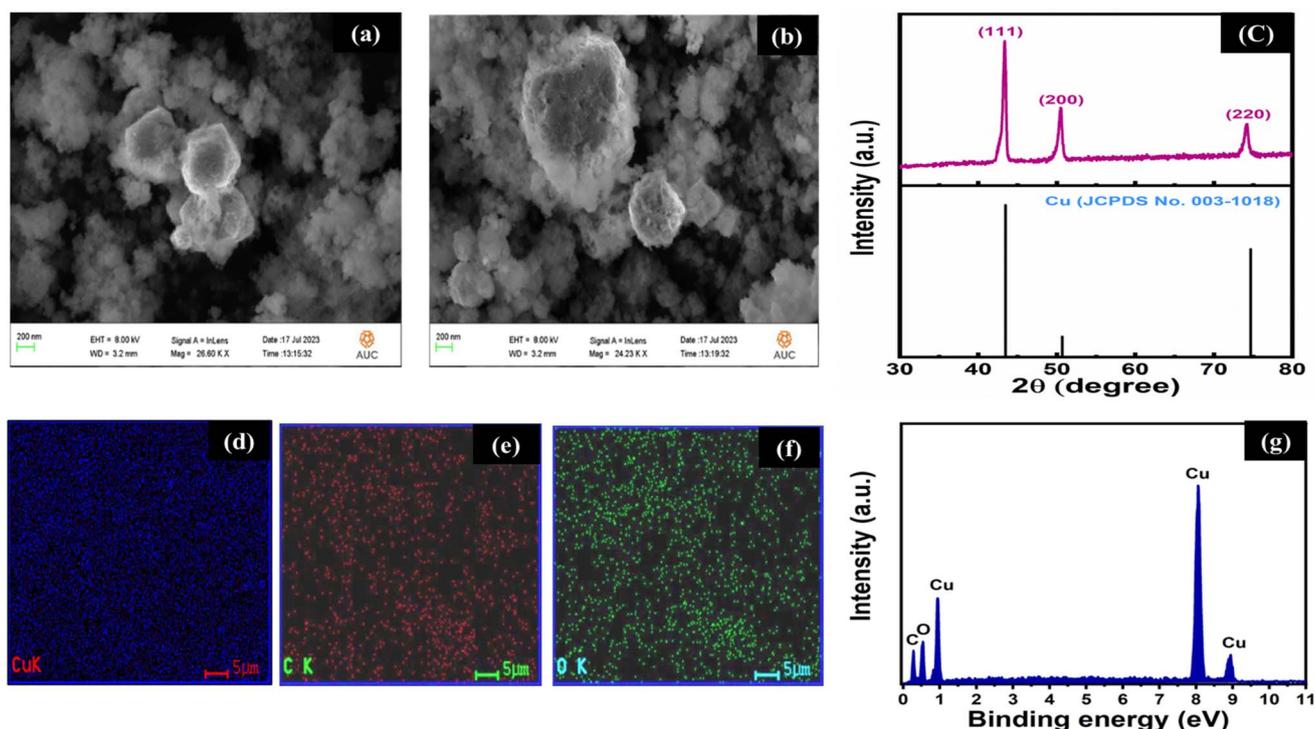
Fig. 1 (a and b) FESEM images, (c) XRD pattern (with a slandered index of Cu, C, O) of the synthesized material, (d–f) EDX elemental mapping, and (g) the corresponding EDX spectrum.

nanoparticles surrounded by a shell of carbon. The nanoparticles have a morphology composed of nanospheres with a size range of 5–20 nm, as presented in Fig. 2a and b. The core–shell of carbon surrounding copper is depicted in Fig. 2c. Moreover, the SAED pattern of the nanoparticles shows the number of rings pointing to the crystalline nature of the Cu as shown in Fig. 2d. The diffraction pattern showed the planes of (111), (200), and (220), corresponding to Cu NPs. The diffraction pattern confirmed the XRD findings. The counter anion in the wet chemistry procedure used to synthesize these particles (citrate) plays a significant role in determining the size of the produced copper nanoparticle along with the alkaline reaction medium and the method by which the reductant is added to the reaction mixture. Additionally, these anions stabilize metal nanoparticle formation, leading to higher yields.[28] The encapsulated Cu material usually fills in the hollow carbon sphere entirely. XRD clearly identified the encapsulated material as elemental Cu. This means carbides and oxides are not contained in the final structure (Cu) and probably do not play any role in their formation process. The shell, composed of

amorphous carbon, plays a significant role as a reducing agent and effectively prevents the formation of oxides.[29,30]

The Raman spectroscopy analysis of the Cu/C NPs (Fig. 3a) revealed two main peaks at 250 and 375 cm^{-1}, which can be ascribed to copper. Additionally, the characteristic graphitic (G) and disorder (D) bands corresponding to carbon are identified at 1398 and 1582 cm^{-1}.[31–33] The D band is linked to carbon atoms with sp^3 hybridization, while the G band arises from the vibrational properties of sp^2 bonded carbon atoms arranged in a 2D hexagonal lattice.[33,34] Simultaneously, the D band indicates a certain degree of structural disorder within the carbon component. The significant I_D/I_G ratio of 1.59 suggests a substantial level of disorder.[35] This disorder could be due to structural defects, vacancies, or the presence of amorphous carbon.[36] The two distinguished peaks are possibly associated with the inherent vibrational modes of Cu atoms or interaction effects in the Cu/C NPs.[37,38]

The identification of functional groups of the Cu/C was performed by FTIR analysis in the range of 500 and 3500 cm^{-1}. The FTIR peaks exhibit characteristic intensities associated with each functional group vibration, Fig. 3b. The observed peaks correspond to O–H groups (3404 cm^{-1}), likely from the vibrations of functional groups due to the presence of free hydroxyl groups on the carbon surface, C–H vibrations (2921 cm^{-1}), C=C stretching vibrations or bending vibrations of absorbed water (1608 cm^{-1}), C–O stretching (1390 cm^{-1}). No absorption peak was detected within the range of 700–500 cm^{-1}, confirming that copper in the Cu nanospheres is in a metallic state, consistent with the findings from the XRD analysis, and not in the form of an oxide.[27,30,39]

Table 1 Weight percentage (wt%) of the elements based on the EDX analysis

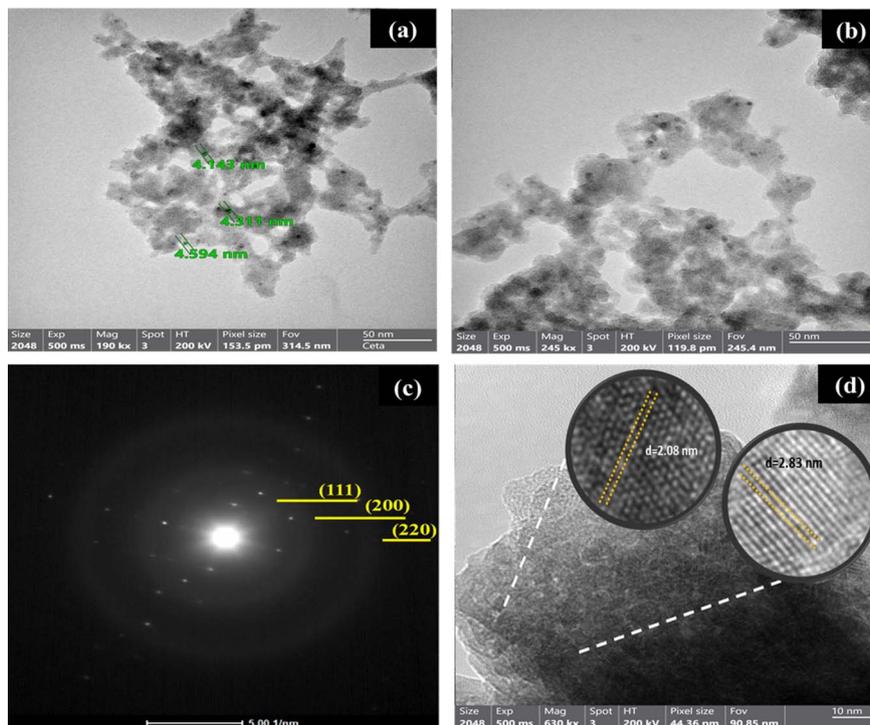| Element	Weight (%)
Copper (Cu)	70%
Carbon (C)	22%
Oxygen (O)	8%

Fig. 2 (a and b) TEM images and (c and d) selected area electron diffraction pattern of the prepared material.
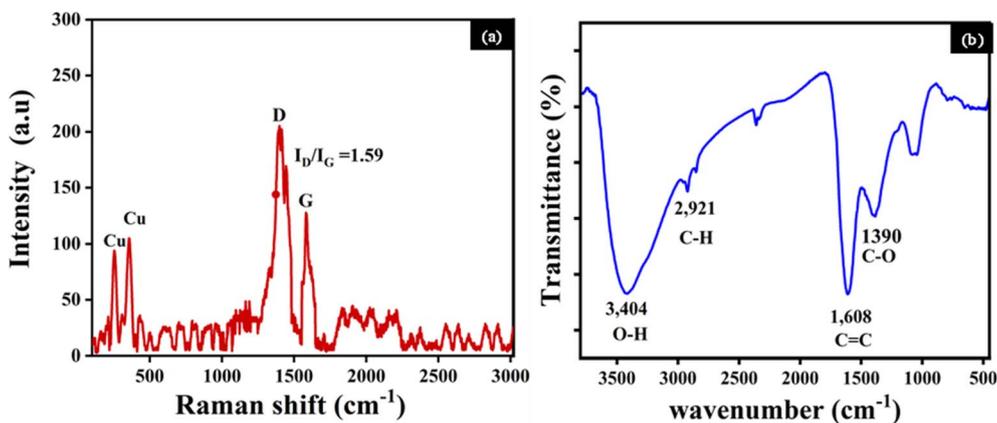

Fig. 3 (a) Raman and (b) FTIR spectra of the fabricated Cu/C NPs.

3.2 Antibacterial assays

To investigate the antibacterial activity of the synthesized Cu/C NPs, a simple colony counts reduction assay of either *E. coli* or *S. aureus* in the presence of a primitive Cu/C NPs concentration (500 μg mL^{-1}) was conducted. The results demonstrated complete inhibition of *E. coli* and a 98% reduction of the number of *S. aureus* colonies as compared to the positive control Fig. 4, with a statistically significant difference ($p < 0.0001$) for both bacterial strains. To get more quantitative insights into the antibacterial efficacy of Cu/C NPs, the MICs against both *E. coli* and *S. aureus* were determined using a plate microdilution method in 96-well plates, Fig. 5. The MICs were evaluated at different bacterial concentrations (high,

intermediate, and low) to assess the impact of bacterial concentration on the MIC. This analysis provides valuable information about the essential nanoparticle concentration for various applications with different bacterial loads.

For *E. coli*, the MIC was found to be 250 μg mL^{-1} at low and intermediate bacterial concentrations and 375 μg mL^{-1} at high bacterial concentrations. *S. aureus* exhibited higher and more concentration-dependent MIC values of 375 μg mL^{-1} at low bacterial concentration, 500 μg mL^{-1} at intermediate bacterial concentration, and 750 μg mL^{-1} at high CFU concentration. The MIC results elucidate the findings of the CFU reduction assay, performed at a high bacterial concentration and 500 μg mL^{-1} of Cu/C NPs. This concentration fell above the MIC for *E. coli* and
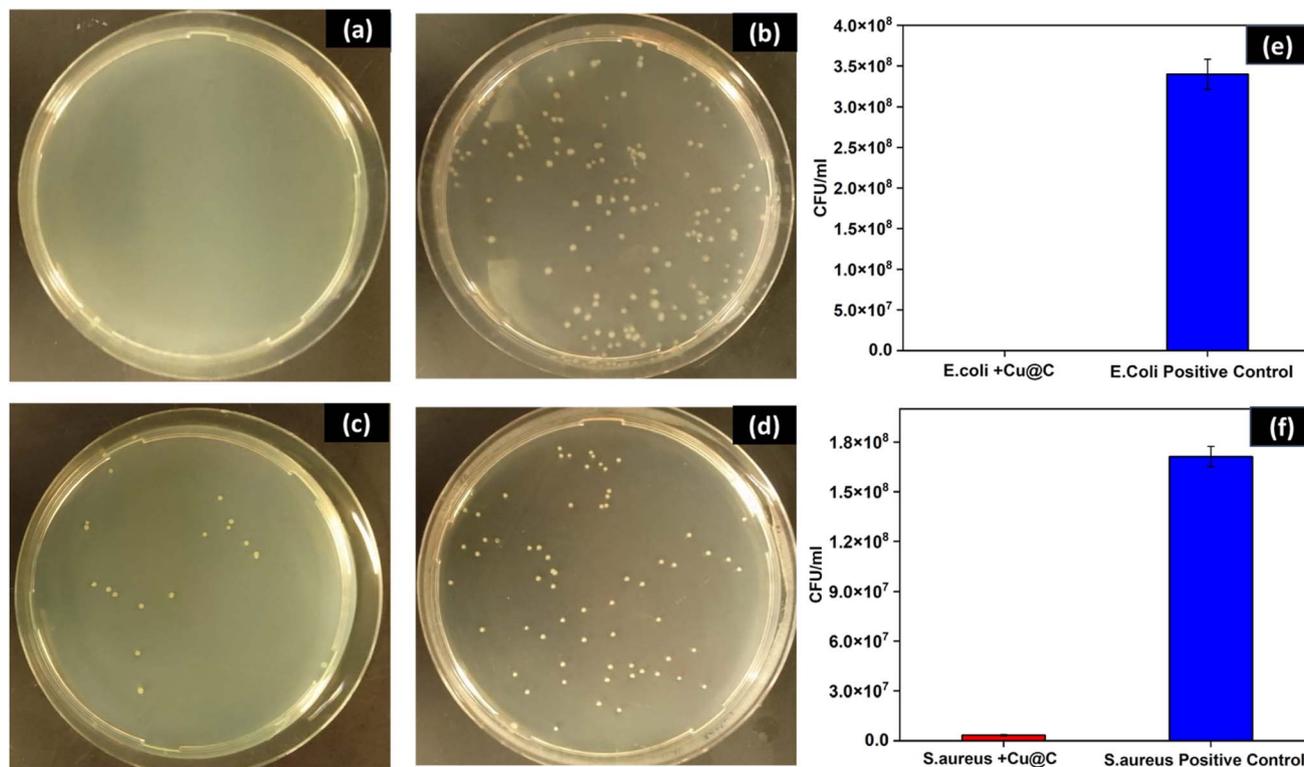
Fig. 4 CFU count of (a) *E. coli* and (b) *S. aureus* treated with 500 μg mL^{-1} of Cu/C NPs at 10^{-4} dilution, alongside positive control plates of (c) *E. coli* and (d) *S. aureus* at 10^{-5} dilution. The corresponding bar graphs of the colony count of (e) *E. coli* (f) *S. aureus*. All experiments were conducted in triplicates, and data is presented as mean and standard deviation.
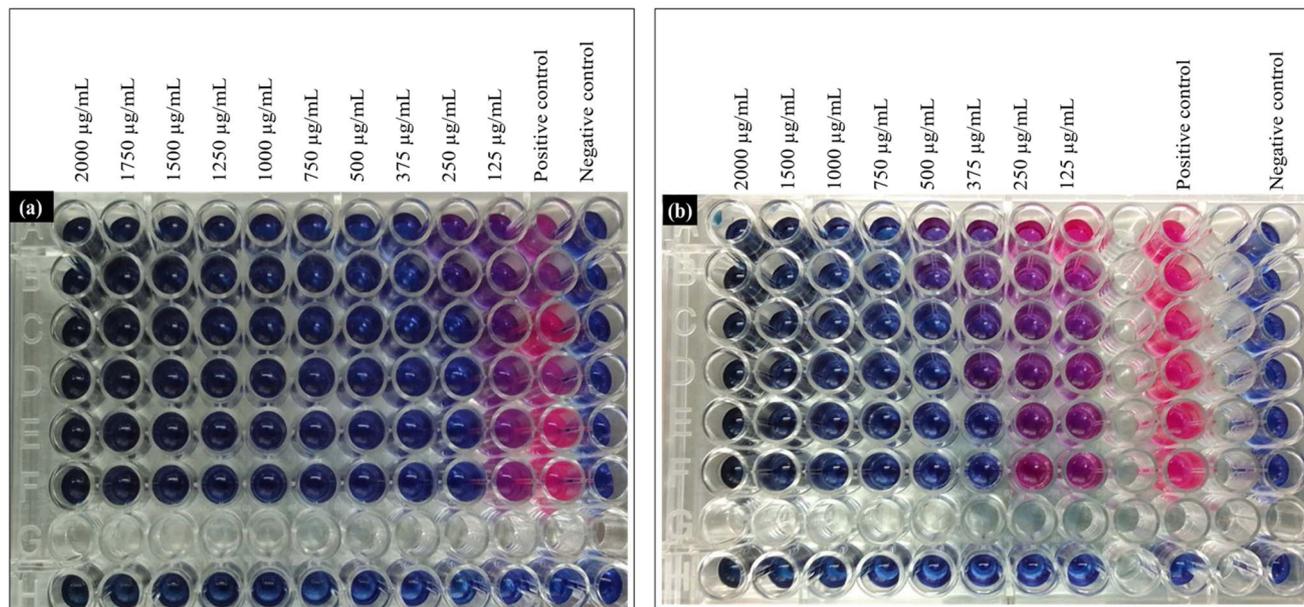

Fig. 5 Resazurin-enhanced MIC determination of Cu/C NPs against (a) *E. coli* and (b) *S. aureus* at high concentration (rows A and B), intermediate concentration (rows C and D), low concentration (rows E and F). Rows H are sterility controls.

below that of *S. aureus*. As a result, *S. aureus* demonstrated partial inhibition, whereas *E. coli* exhibited complete inhibition. Similarly, Chen *et al.* reported higher MIC for Cu NPs

encapsulated by carbon in the case of *S. aureus* as compared to *E. coli*.[40] In addition, previous studies reported that the antibacterial efficacy of copper-doped carbon dots was better in the
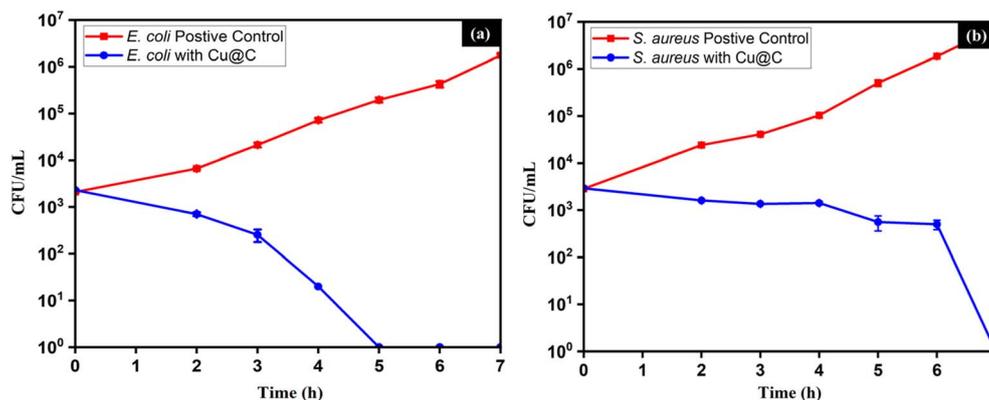
Fig. 6 Time−kill curve for (a) *E. coli* and (b) *S. aureus* incubated with Cu/C NPs (1000 μg mL^{-1}) as compared to the bacterial growth curves of their positive controls. Data are presented as means ± standard deviations (error bars).

Table 2 Percentages of reduction of the initial inocula of both *E. coli* and *S. aureus* treated with 1000 μg mL^{-1} Cu/C NPs at different time points

Time, h	CFU reduction of *E. coli*	CFU reduction of *S. aureus*
2	69.36%	45.05%
3	89.02%	53.58%
4	99.13%	51.54%
5	100.00%	80.89%
6	100.00%	82.94%
7	100.00%	100.00%

case of *E. coli* as compared to *S. aureus*.[41,42] This can be attributed to the difference in the cell wall structure of the two bacteria. The copper cations can be attracted to the electronegative charges of lipopolysaccharides and teichoic acid on the surfaces of *E. coli* and *S. aureus*, respectively. However, the thick peptidoglycan layer of the Gram-positive *S. aureus* can decrease the rate of penetration of the cations inside the cell, which is a probable explanation for why *S. aureus* requires more Cu/C NPs concentration to be inhibited.[43]

Time–kill analyses against *E. coli* and *S. aureus* were undertaken to get insights into the bactericidal kinetics of Cu/C NPs. This included the counting of CFU at different time intervals,

Table 3 Antibacterial activity of different copper-based nanoparticles extracted from e-waste[a]

Paper	Source of copper	Bacterial species	Antibacterial assay	Results
Current study	WPCBs	*S. aureus* *E. coli*	Resazurin enhanced broth microdilution assay	MICs for *E. coli* ranged from 200 to 375 μg mL^{-1}, and MICs for *S. aureus* ranged from 375 to 750 μg mL^{-1} according to the bacterial load
Abdelbasir *et al.*[44]	WPCBs	*B. cereus* *S. aureus* *E. coli* *S. typhi* *P. aeruginosa*	Disk diffusion method	ZOIs (in mm) were 16.8 ± 1.53 for *B. cereus*, 9.0 ± 1.00 for *S. aureus*, 12.7 ± 1.04 for *E. coli*, 10.3 ± 0.76 for *S. typhi*, and 9.3 ± 0.76 for *P. aeruginosa*
Tatariants *et al.*[21]	MB, VC, and RAM	*E. coli* *S. aureus* *P. aeroginosa*	Broth microdilution method	RAM- derived CuNPs had MIC of about 3% against the three bacterial strains – both MB- and VC- derived CuNPs had MICs were not detectable (above 6%)
Sinha *et al.*[45]	WPCBs	*E. coli*	Well diffusion method	ZOI was equal to 13.5 mm
Majumder *et al.*[46]	Integrated circuits on electronic boards	*E. coli*	Disk diffusion method	ZOI was equal to 5 mm

[a] MIC: minimum inhibitory concentration; ZOI: zone of inhibition; WPCB: waste printed circuit boards; CuNPs: copper nanoparticles; MB: motherboard; VC: video card; RAM: random access memory; *S. aureus*: Staphylococcus aureus; *E. coli*: Escherichia coli; *B. cereus*: Bacillus cereus; *S. typhi*: Salmonella typhi; *P. aeruginosa*: Pseudomonas aeruginosa.

Fig. 6. Moreover, the degrees of reduction in CFU number compared to the initial inoculation were measured as percentages at different time intervals, Table 2.

The bactericidal kinetics of *E. coli* was faster than that of *S. aureus*, achieving complete eradication of bacteria after five and seven hours, respectively. Moreover, the curves for the two organisms followed different trends. In the case of *E. coli*, the natural logarithm of CFU counts was fit to an exponential decay model through regression analysis, as described by eqn (2):

$$\ln CFU_E = -1.9025 \, t + 10.282 \tag{2}$$

CFU_E refers to CFU mL^{-1} of *E. coli* samples treated by Cu/C NPs at a distinct time point (t). The time coefficient is the rate constant (k) of bactericidal activity. The *R*-squared value was estimated at 0.947, indicating a perfect fit for the model. On the other hand, the trend of CFU reduction over time in the case of *S. aureus* exhibited a gradual decline with two-time plateaus, one between 3 and 4 hours time points and the other between 5 and 6 hours time points. Therefore, the regression analysis failed to fit an exponential decay model. However, 100% elimination of *S. aureus* was achieved in as few as seven hours, making Cu/C NPs a promising antibacterial agent that can be implemented in materials and surfaces. The extraction of Cu/C NPs from waste, coupled with its application in antibacterial materials, not only brings about economic and environmental benefits but also serves as a promising material for further exploration in related applications.

Our e-waste-derived Cu/C NPs showed MIC of 250 μg mL^{-1} against *E. coli*, and 375 μg mL^{-1} against *S. aureus* at bacterial load of 1×10^3 to 1×10^4 CFU mL^{-1}. These results indicate that our Cu/C NPs are significantly more effective antibacterial agents than Cu NPs reported in the literature, see Table 3. Note that a direct comparison with the studies by Abdelbasir *et al.*,[44] Sinha *et al.*,[45] and Majumder *et al.*[46] (Table 3) is not possible, as they employed qualitative agar diffusion assays rather than the quantitative MIC method. The extraction of Cu/C NPs from e-waste, coupled with their application in antibacterial materials, not only brings about economic and environmental benefits, but also serves as a promising material for further exploration in related applications.

4. Conclusion

This study successfully demonstrated the recovery of Cu/C NPs from e-waste for antibacterial applications. The synthesized nanoparticles showed well-defined, uniform spherical copper NPs, within carbon matrix. The characterization results confirmed the purity and composition of the nanoparticles. Antibacterial assays and bactericidal kinetics revealed significant antibacterial activity against both *E. coli* and *S. aureus*, with Cu/C NPs showing quite more potent effect on *E. coli*. Specifically, Cu/C NPs (500 μg mL^{-1}) caused 100% and 98% reduction of the CFU counts of *E. coli* and *S. aureus*, respectively. MICs ranged from 200 to 375 μg mL^{-1} for *E. coli* and 375 to 750 μg mL^{-1} for *S. aureus*, depending on the bacterial load. Additionally, Cu/C NPs (1000 μg mL^{-1}) caused the complete elimination of *E. coli* and *S. aureus* after five and seven hours, respectively. The findings suggest the potential of utilizing electronic waste as a valuable resource for producing antibacterial materials. The environmentally friendly synthesis process and the demonstrated antibacterial properties of Cu/C NPs make these nanoparticles promising candidates for applications in antibacterial materials and surfaces.

Data availability

The data supporting this article can be provided upon request.

Conflicts of interest

There are no conflicts to declare.

References

1 V. Forti, C. P. Baldé, R. Kuehr and G. Bel, *The Global E-waste Monitor Quantities, Flows and the Circular Economy Potential*, United Nations University (UNU)/United Nations Institute for Training and Research (UNITAR) – co-hosted SCYCLE Programme, International Telecommunication Union (ITU) & International Solid Waste Association (ISWA), Bonn/Geneva/Rotterdam, 2020.

2 D. N. Perkins, M. B. Drisse, T. Nxele and P. D. Sly, *Ann. Glob. Health*, 2014, **80**, 286–295.

3 A. Kumar, M. Holuszko and D. C. R. Espinosa, *Resour., Conserv. Recycl.*, 2017, **122**, 32–42.

4 V. Sahajwalla and R. Hossain, *Mater. Today Sustain.*, 2020, **9**, 100040.

5 A. Gurgul, W. Szczepaniak and M. Zabłocka-Malicka, *Sci. Total Environ.*, 2018, **624**, 1119–1124.

6 R. Seif, F. Zakaria and N. K. Allam, *Environ. Dev. Sustain.*, 2024, **26**, 5473–5508.

7 S. M. Abdelbasir, D. A. Rayan and M. M. Ismail, *Environ. Sci. Pollut. Res.*, 2023, **30**, 89690–89704.

8 M. M. Abdelkhalek, A. M. Mohamed, R. Z. Abdallah, G. E. Khedr, R. Siam and N. K. Allam, *Nanoscale Adv.*, 2024, **6**, 3355–3366.

9 A. Dubey, A. Singh, A. Ahmed, A. K. Sundramoorthy, S. P. Patole and S. Arya, *Surf. Interfaces*, 2024, **51**, 104731.

10 A. Dubey, A. Singh, A. Sharma, A. K. Sundramoorthy, R. Mahadeva, V. Gupta, S. Dixit and S. Arya, *Appl. Phys. A*, 2023, **129**, 1–14.

11 S. B. Mayegowda, A. Roy, N. G. Manjula, S. Pandit, S. Alghamdi, M. Almehmadi, M. Allahyani, N. S. Awwad and R. Sharma, *Front. Cell. Infect. Microbiol.*, 2023, **13**, 1224778.

12 A. M. Mohamed, W. A. Abbas, G. E. Khedr, W. Abass and N. K. Allam, *Sci. Rep.*, 2022, **12**, 15989.

13 L. P. Arendsen, R. Thakar and A. H. Sultan, *Clin. Microbiol. Rev.*, 2019, **32**, e00125.

14 S. B. Rana, R. P. P. Singh and S. Arya, *J. Mater. Sci.: Mater. Electron.*, 2017, **28**, 2660–2672.

15 M. L. Ermini and V. Voliani, *ACS Nano*, 2021, **15**, 6008–6029.

16 E. O. Mikhailova, *J. Funct. Biomater.*, 2020, **11**, 84.

17 A. N. El-Shazly, G. S. El-Sayyad, A. H. Hegazy, M. A. Hamza, R. M. Fathy, E. T. El Shenawy and N. K. Allam, *Sci. Rep.*, 2021, **11**, 5609.

18 M. Bhagat, S. Rajput, S. Arya, S. Khan and P. Lehana, *Bull. Mater. Sci.*, 2015, **38**, 1253–1258.

19 P. Chen, P. Zhang, Y. Cui, X. Fu and Y. Wang, *Mater. Today Sustain.*, 2023, **21**, 100276.

20 M. Bhagat, R. Anand, R. Datt, V. Gupta and S. Arya, *J. Inorg. Organomet. Polym. Mater.*, 2019, **29**, 1039–1047.

21 M. Tatariants, S. Yousef, S. Sakalauskaitė, R. Daugelavičius, G. Denafas and R. Bendikiene, *Waste Manage.*, 2018, **78**, 521–531.

22 R. V. Murugan, G. Sridharan, R. Atchudan, S. Arya, D. Nallaswamy and A. Sundramoorthy, *Curr. Nanosci.*, 2024, **20**, 1–10.

23 D. M. Elsayed, S. M. Abdelbasir, H. M. Abdel-Ghafar, B. A. Salah and S. A. Sayed, *J. Environ. Chem. Eng.*, 2020, **8**, 103826.

24 J. Xiong, Y. Wang, Q. Xue and X. Wu, *Green Chem.*, 2011, **13**, 900–904.

25 S. Cavalheiro, A. Beatriz, B. Pruski, S. Buchhorn, D. F. Suzane, O. Allend and D. D. Hartwig, *Mol. Biol. Rep.*, 2020, **47**, 9615–9625.

26 S. Foerster, V. Desilvestro, L. J. Hathaway, C. L. Althaus and M. Unemo, *J. Antimicrob. Chemother.*, 2017, **72**, 1961–1968.

27 A. M. Abdelmohsen, A. M. Agour, I. M. Badawy, G. E. Khedr, Y. I. Mesba and N. K. Allam, *Sustainable Energy Fuels*, 2024, DOI: 10.1039/D4SE00700J.

28 R. Seif El-Nasr, S. M. Abdelbasir, A. H. Kamel and S. S. M. Hassan, *Sep. Purif. Technol.*, 2020, **230**, 115860.

29 M. M. Hasan, G. E. Khedr, F. Zakaria and N. K. Allam, *ACS Appl. Energy Mater.*, 2022, **5**, 9692–9701.

30 A. M. Agour, E. Elkersh, G. E. Khedr, H. G. El-Aqapa and N. K. Allam, *ACS Appl. Nano Mater.*, 2023, **6**, 15980–15989.

31 A. C. Ferrari and D. M. Basko, *Nat. Nanotechnol.*, 2013, **8**, 235–246.

32 H. A. Ghaly, A. G. El-Deen, E. R. Souaya and N. K. Allam, *Electrochim. Acta*, 2019, **310**, 58–69.

33 A. S. Hassanien, R. A. Shedeed and N. K. Allam, *J. Phys. Chem. C*, 2016, **120**, 21678–21684.

34 J. Maultzsch, S. Reich and C. Thomsen, *Phys. Rev. B: Condens. Matter Mater. Phys.*, 2004, **70**, 1–9.

35 M. Samir, M. Salama and N. K. Allam, *J. Mater. Chem. A*, 2016, **4**, 9375–9380.

36 L. M. Malard, M. A. Pimenta, G. Dresselhaus and M. S. Dresselhaus, *Phys. Rep.*, 2009, **473**, 51–87.

37 J. Yan, Y. Zhang, P. Kim and A. Pinczuk, *Phys. Rev. Lett.*, 2007, **98**, 166802.

38 B. Kumar, D. K. Verma, A. K. Singh, V. Kavita, N. Shukla and R. B. Rastogi, *Compos. Interfaces*, 2020, **27**, 777–794.

39 G. Jozanikohan and M. N. Abarghooei, *J. Pet. Explor. Prod. Technol.*, 2022, **12**, 2093–2106.

40 H. Chen, J. Wu, M. Wu and H. Jia, *N. Carbon Mater.*, 2019, **34**, 382–389.

41 H. Wang, N. Wang, H. Quan, F. Zhang, J. Fan, H. Feng, M. Cheng, Z. Liao, X. Wang and Y. Xiang, *Agric. Water Manag.*, 2022, **269**, 107645.

42 F. W. Liu, T. M. Cheng, Y. J. Chen, K. C. Yueh, S. Y. Tang, K. Wang, C. L. Wu, H. S. Tsai, Y. J. Yu, C. H. Lai, W. S. Chen and Y. L. Chueh, *Sol. Energy Mater. Sol. Cells*, 2022, **241**, 111691.

43 Y. Wang, J. Yao, Z. Cao, P. Fu, C. Deng, S. Yan, S. Shi and J. Zheng, *Chem.—Eur. J.*, 2022, **28**, e202104174.

44 S. M. Abdelbasir, D. A. Rayan and M. M. Ismail, *Environ. Sci. Pollut. Res.*, 2023, **30**, 89690–89704.

45 R. Sinha, G. Chauhan, A. Singh, A. Kumar and S. Acharya, *J. Environ. Chem. Eng.*, 2018, **6**, 1053–1061.

46 D. R. Majumder, *Int. J. Eng. Sci. Technol.*, 2012, **4**, 4380–4389.